

University of Wollongong

Research Online

---

Australian Institute for Innovative Materials -  
Papers

Australian Institute for Innovative Materials

---

1-1-2014

## Photocatalytic degradation of methyl orange by CeO<sub>2</sub> and Fe-doped CeO<sub>2</sub> films under visible light irradiation

D Channei  
*Chiang Mai University*

B Inceesungvorn  
*Chiang Mai University*

N Wetchakun  
*Chiang Mai University*

S Ukritnukun  
*University of New South Wales*

Andrew Nattestad  
*University of Wollongong, anattest@uow.edu.au*

*See next page for additional authors*

Follow this and additional works at: <https://ro.uow.edu.au/aiimpapers>

 Part of the [Engineering Commons](#), and the [Physical Sciences and Mathematics Commons](#)

---

### Recommended Citation

Channei, D; Inceesungvorn, B; Wetchakun, N; Ukritnukun, S; Nattestad, Andrew; Chen, Jun; and Phanichphant, S, "Photocatalytic degradation of methyl orange by CeO<sub>2</sub> and Fe-doped CeO<sub>2</sub> films under visible light irradiation" (2014). *Australian Institute for Innovative Materials - Papers*. 1203.  
<https://ro.uow.edu.au/aiimpapers/1203>

Research Online is the open access institutional repository for the University of Wollongong. For further information contact the UOW Library: [research-pubs@uow.edu.au](mailto:research-pubs@uow.edu.au)

---

# Photocatalytic degradation of methyl orange by CeO<sub>2</sub> and Fe-doped CeO<sub>2</sub> films under visible light irradiation

## Abstract

Undoped CeO<sub>2</sub> and 0.50-5.00 mol% Fe-doped CeO<sub>2</sub> nanoparticles were prepared by a homogeneous precipitation combined with homogeneous/impregnation method, and applied as photocatalyst films prepared by a doctor blade technique. The superior photocatalytic performances of the Fe-doped CeO<sub>2</sub> films, compared with undoped CeO<sub>2</sub> films, was ascribed mainly to a decrease in band gap energy and an increase in specific surface area of the material. The presence of Fe<sup>3+</sup> as found from XPS analysis, may act as electron acceptor and/or hole donor, facilitating longer lived charge carrier separation in Fe-doped CeO<sub>2</sub> films as confirmed by photoluminescence spectroscopy. The 1.50 mol% Fe-doped CeO<sub>2</sub> film was found to be the optimal iron doping concentration for MO degradation in this study.

## Keywords

light, photocatalytic, degradation, methyl, orange, irradiation, ceo2, visible, fe, doped, films, under

## Disciplines

Engineering | Physical Sciences and Mathematics

## Publication Details

Channei, D., Inceesungvorn, B., Wetchakun, N., Ukritnukun, S., Nattestad, A., Chen, J. & Phanichphant, S. (2014). Photocatalytic degradation of methyl orange by CeO<sub>2</sub> and Fe-doped CeO<sub>2</sub> films under visible light irradiation. *Scientific Reports*, 4 1-7.

## Authors

D Channei, B Inceesungvorn, N Wetchakun, S Ukritnukun, Andrew Nattestad, Jun Chen, and S Phanichphant



OPEN

CONFERENCE  
PROCEEDINGSAPEnergy2014  
.....SUBJECT AREAS:  
NANOPARTICLES  
NANOSCIENCE AND  
TECHNOLOGYReceived  
21 February 2014Accepted  
27 June 2014Published  
29 August 2014Correspondence and  
requests for materials  
should be addressed to  
S.P. (sphanichphant@  
yahoo.com) or A.N.  
(anattest@uow.edu.  
au)

# Photocatalytic Degradation of Methyl Orange by CeO<sub>2</sub> and Fe-doped CeO<sub>2</sub> Films under Visible Light Irradiation

D. Channei<sup>1</sup>, B. Inceesungvorn<sup>1</sup>, N. Wetchakun<sup>2</sup>, S. Ukritnukun<sup>3</sup>, A. Nattestad<sup>4</sup>, J. Chen<sup>4</sup>  
& S. Phanichphant<sup>5</sup>

<sup>1</sup>Department of Chemistry, Faculty of Science, Chiang Mai University, Chiang Mai 50200, Thailand, <sup>2</sup>Department of Physics and Materials Science, Faculty of Science, Chiang Mai University, Chiang Mai 50200, Thailand, <sup>3</sup>School of Materials Science and Engineering, University of New South Wales, Sydney, NSW 2052, Australia, <sup>4</sup>Intelligent Polymer Research Institute, ARC Centre of Excellence for Electromaterials Science, Australian Institute of Innovative Materials, University of Wollongong, Wollongong, NSW 2522, Australia, <sup>5</sup>Materials Science Research Center, Faculty of Science, Chiang Mai University, Chiang Mai 50200, Thailand.

Undoped CeO<sub>2</sub> and 0.50–5.00 mol% Fe-doped CeO<sub>2</sub> nanoparticles were prepared by a homogeneous precipitation combined with homogeneous/impregnation method, and applied as photocatalyst films prepared by a doctor blade technique. The superior photocatalytic performances of the Fe-doped CeO<sub>2</sub> films, compared with undoped CeO<sub>2</sub> films, was ascribed mainly to a decrease in band gap energy and an increase in specific surface area of the material. The presence of Fe<sup>3+</sup> as found from XPS analysis, may act as electron acceptor and/or hole donor, facilitating longer lived charge carrier separation in Fe-doped CeO<sub>2</sub> films as confirmed by photoluminescence spectroscopy. The 1.50 mol% Fe-doped CeO<sub>2</sub> film was found to be the optimal iron doping concentration for MO degradation in this study.

Organic pollutants from the textile industry represent a major source of water contamination. About 15% of commercially used dyes are released without treatment<sup>1</sup>, while those that are required either a chemical or energy intensive processing which leads to further strain on the environment. An inherent requirement of most of these dyes is that they are stable for long periods of time in their application. Unfortunately, this also makes degradation (particularly biodegradation) of their excess difficult. Methyl orange (MO) is a simple azo dye. Azo dyes are widely used in textile, printing, pharmaceutical, and research laboratories. It can enter the human body through skin, and can cause the death of lung tissues, fast heart rate, and vomiting<sup>2</sup>. For these reasons, MO was chosen as a model dye for photocatalytic degradation in this research.

Advanced oxidation processes based on semiconductor oxide photocatalysts are an effective method for dye degradation<sup>3</sup>, with various oxide semiconductors such as TiO<sub>2</sub>, ZnO, and WO<sub>3</sub> being used in heterogeneous photocatalysis<sup>4–6</sup>. CeO<sub>2</sub> has been shown to be a particularly effective catalyst, in part due to the redox potential of the Ce<sup>4+</sup>/Ce<sup>3+</sup> couple, as well as its resistance to chemical and photocorrosion, and strong light absorption in the UV region (absorption edge ~385–400 nm). Unfortunately the large band gap (~3.2 eV) limits further application of CeO<sub>2</sub><sup>7–8</sup>. From the AM1.5 spectrum, it can be seen that UV light only composes ~3–5% of the photon flux reaching the earth's surface, while around 45% is in the visible light range. Thus it would be hugely beneficial to extend the light absorption of CeO<sub>2</sub> to the visible light region<sup>9</sup>, and as such, many methods have been investigated to shift the absorption onset by doping or coupling with other materials<sup>10,11</sup>.

Doping with metal ions, specially Fe<sup>3+</sup> was chosen in this research as it is believed to facilitate the Fenton reaction, which help improve the photocatalytic activity by producing the very powerful hydroxyl radicals (OH<sup>•</sup>) as oxidizers<sup>12,13</sup>.

The separation of catalyst from the waste water suspension is another major problem which limits practical application of nanomaterials<sup>14,15</sup>. Dense films lack the high surface area required for effective catalysis. Therefore, the CeO<sub>2</sub> nanoparticles are fabricated to form a mesoporous film. The doctor blade deposition technique was employed for film preparation to well adhered, high surface, porous films with a good photocatalytic activity<sup>16,17</sup>.

In this study, kinetics studies of the photocatalytic degradation of MO over Fe-doped CeO<sub>2</sub> films were investigated. Improved electron-hole separation and charge transfer process mechanism was also proposed based on the obtained XPS and UV-vis DRS results. Also the formation of OH<sup>•</sup> in the photocatalytic process has been confirmed via photoluminescence spectroscopy.

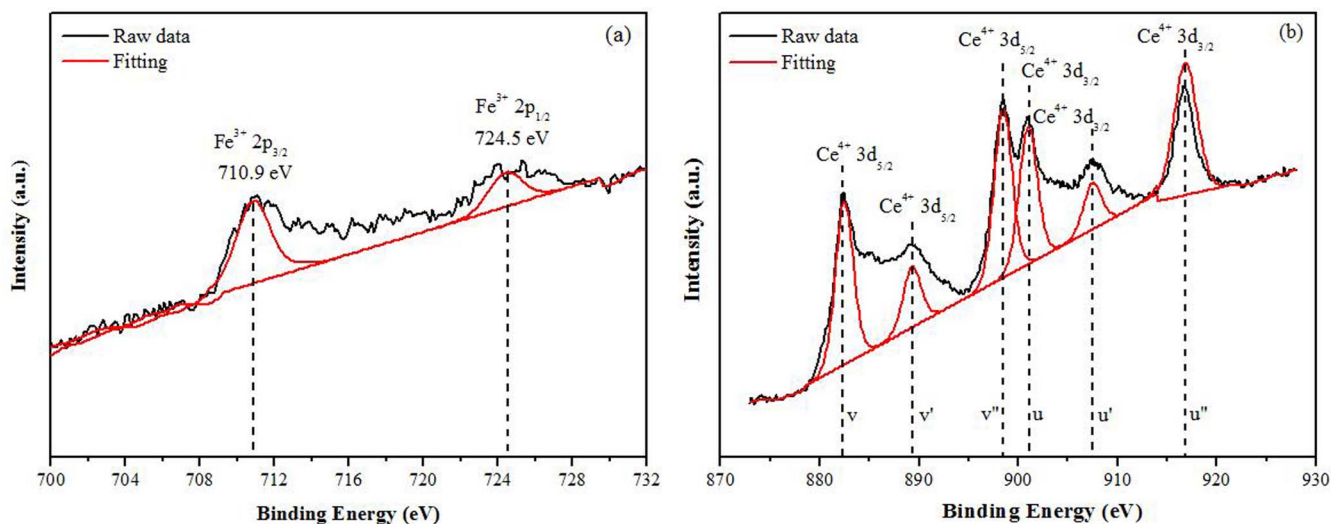


**Figure 1** | The XPS spectra of 5.00 mol% Fe-doped CeO<sub>2</sub> (a) Fe 2p and (b) Ce 3d.

XPS analysis was carried out in order to characterise the valence states of both cerium and iron (5.00 mol% Fe-doped CeO<sub>2</sub>). The two main peaks of Fe 2p in Figure 1a were observed at 710.9 and 724.5 eV of 2p<sub>3/2</sub> and 2p<sub>1/2</sub> respectively, which corresponds with the Fe<sup>3+</sup> species in Fe<sub>2</sub>O<sub>3</sub><sup>18,19</sup>. For the Ce 3d XPS spectrum, the typical six peaks of Ce 3d are presented in Figure 1b. The peaks denoted as V (882.5 eV), V' (889.3 eV), V'' (898.5 eV), U (901.0 eV), U' (907.5 eV), and U'' (916.8 eV) were attributed to Ce<sup>4+</sup> state<sup>20,21</sup>.

Each of the XRD patterns in Figure 2 indexed as CeO<sub>2</sub>, with a cubic fluorite structure (JCPDS 3403940)<sup>22</sup>. No other peaks from either metallic iron or Fe<sub>x</sub>O<sub>y</sub> were found in the XRD analysis. Samples with higher doping revealed a shift in the peak associated with the 111 direction (located at  $2\theta = 28.3899$  for the undoped sample), which shifted towards higher values. The calculated crystallite size and lattice parameter decreased slightly with increasing iron content. This may be explained by larger Ce<sup>4+</sup> ions (0.101 nm) being replaced by smaller Fe<sup>3+</sup> ions (0.064 nm), thus decreasing the lattice parameters, unit cell volume and crystallite size<sup>23</sup> (Supplementary Information 1).

To obtain the band gap energies of the Fe-doped CeO<sub>2</sub> films, Schuster-Kubelka-Munk absorption function ( $(\infty hv)^{1/n}$ ) was plotted against the photon energy ( $hv$ ) according to equation (1)<sup>24</sup>.

$$(\infty hv)^{1/n} = A(hv - E_g) \quad (1)$$

where A is a proportionality constant,  $h$  is Planck's constant,  $\nu$  is the frequency of vibration (hence  $h\nu$  is photon energy), and  $\infty$  is an absorption coefficient. The value of  $n$  depends on the type of optical transition of the semiconductor ( $n=2$  for indirect transition)<sup>25</sup>. The approximated band gap can then be determined from the straight line x-intercept as shown in Figure 3.

The kinetics of MO decolourisation are presented in Figure 4, and are found to follow pseudo-first order reaction as shown in equation (2)<sup>26</sup>:

$$-\ln(C/C_0) = kt \quad (2)$$

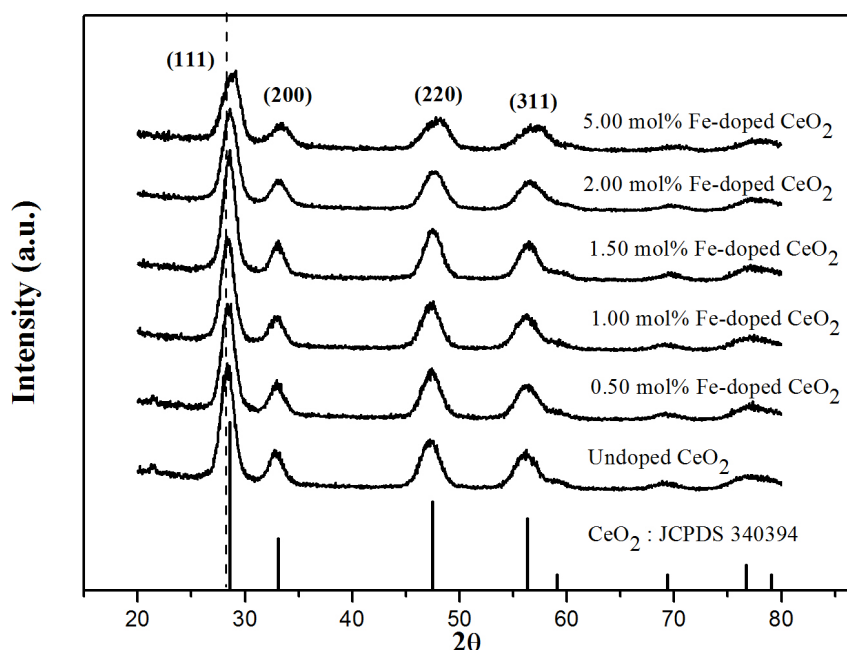


**Figure 2** | XRD patterns of the undoped and Fe-doped CeO<sub>2</sub> films fabricated by the doctor blade technique.

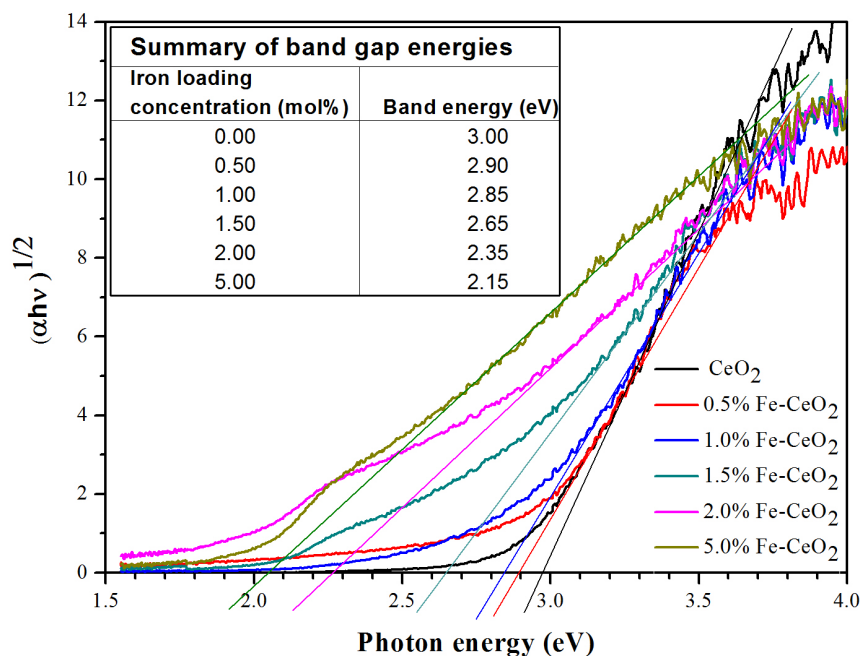


**Figure 3** | Schuster-Kubelka-Munk absorption function of Fe-doped CeO<sub>2</sub> films with an inset showing the band gap energies of catalyst films.

where  $k$  is the apparent rate constant ( $\text{min}^{-1}$ ),  $C_0$  is the initial concentration of dye and  $C$  is the concentration of dye at time ( $t$ ). As the dye concentration in these experiments remains in the regime where the Beer-Lambert law holds, the concentration can be substituted by the dye absorbance at a given wavelength (typically the peak absorption).

Iron modified CeO<sub>2</sub> films clearly presented superior photocatalytic activity towards the degradation of MO in pH 5 conditions compared to undoped CeO<sub>2</sub>, with 1.50 mol% Fe doping providing the most rapid dye degradation. BET analysis (Supplementary Information 2) showed that the 1.50 mol% Fe-doped CeO<sub>2</sub> film possessed the highest specific surface area, and hence more active sites are available for the MO degradation reaction<sup>27</sup>.

Another important real world consideration for photocatalytic systems is long-term stability. The 1.50 mol% Fe-doped CeO<sub>2</sub> was employed to degrade MO solution (pH5) for 2 h before the films was removed and regenerated (heated to 250 °C for 120 min) and process repeated (10 cycles in total). The material displayed good stability with regards to photocatalytic performance, with less than 10% decreased from its initial activity during photodegradation process (Figure 5).

The observation of photoluminescence (PL) was employed to explain the chance of electron-hole pair recombination in catalyst. Since the PL emission spectra was reported from the recombination of excited electrons and holes<sup>28,29</sup>, thus a higher PL intensity indicated a higher recombination rate of electron-hole pairs under light irra-

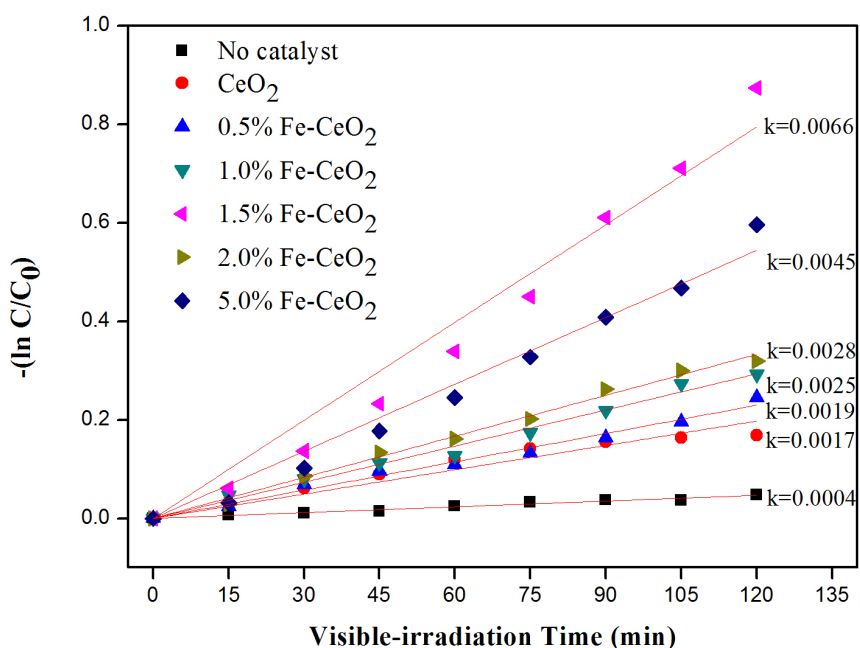


**Figure 4** | The kinetics plots for pseudo first order reaction of MO decolourisation at pH 5.

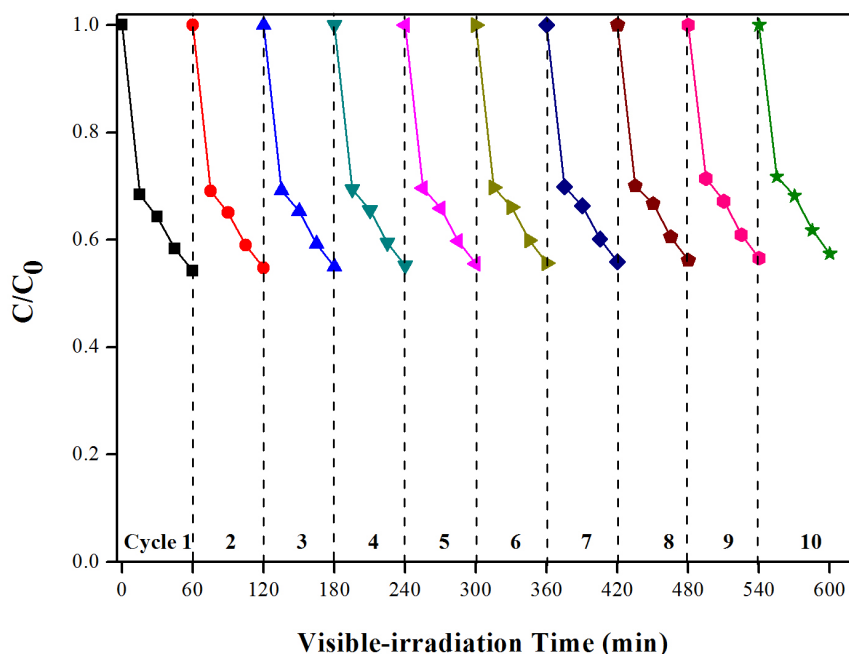


Figure 5 | Cycling runs of MO decolourisation using 1.50 mol% Fe-doped  $\text{CeO}_2$  film at pH 5 of MO solution.

diation. In Figure 6, undoped  $\text{CeO}_2$  presented the highest intensity, which indicated that undoped  $\text{CeO}_2$  provided the fastest recombination rate of electrons and holes. After the iron ions were introduced to  $\text{CeO}_2$ , the intensity of the PL emission gradually decreased, which confirmed that the doping with iron ions could delay the recombination rate of photogenerated charge carriers.

Moreover, the detection of hydroxyl radical ( $\text{OH}^\bullet$ ) in photocatalytic reactions have been reported via the reaction of terephthalic acid (TA) with  $\text{OH}^\bullet$ , and formed the fluorescent 2-hydroxy terephthalate ( $\text{TA-OH}^\bullet$ ) as a reaction product, which can be detected by fluorescence spectroscopy<sup>30</sup>. In this study, the 1.50% Fe-doped  $\text{CeO}_2$  catalyst was employed to detect the generated  $\text{OH}^\bullet$  on the surface. As

shown in Figure 7, the PL intensity at approximately 425 nm of  $\text{TA-OH}^\bullet$  increased in the first hour of photocatalytic degradation process and kept constant with increasing time after this one hour, which means that the catalyst presented the highest performance in the first hour of light irradiation.

### Discussion

Based on the optical band gap energy values determined above (Figure 3) and equation (3) and (4), below, the conduction band (CB) and valence band (VB) potentials of  $\text{CeO}_2$  can be calculated<sup>31</sup>:

$$E_{\text{cb}}(\text{CeO}_2) = \chi(\text{CeO}_2) - E^{\text{C}} - \frac{1}{2} E_{\text{g}} \quad (3)$$

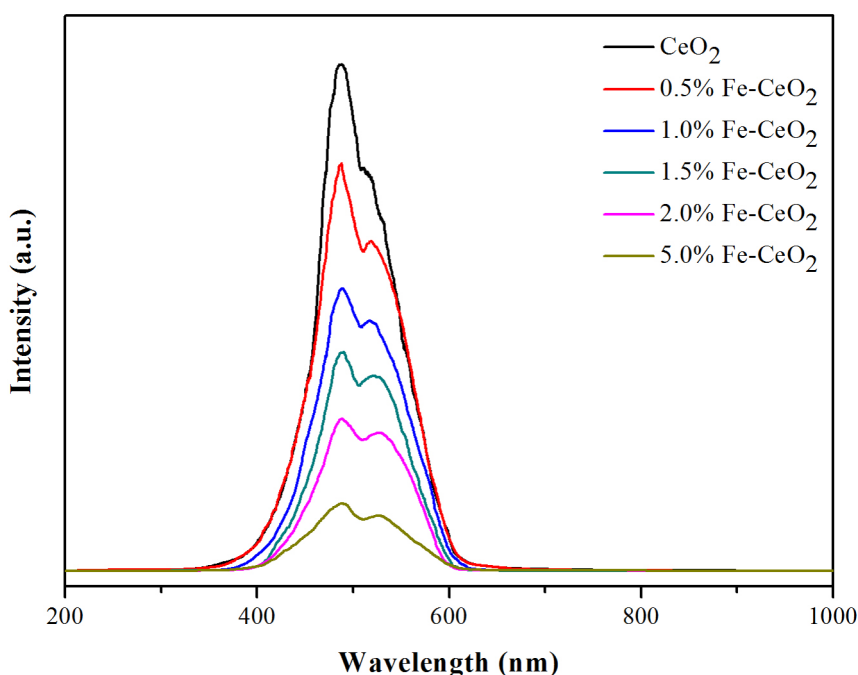


Figure 6 | PL spectra of  $\text{CeO}_2$  at different amounts of iron doping level.



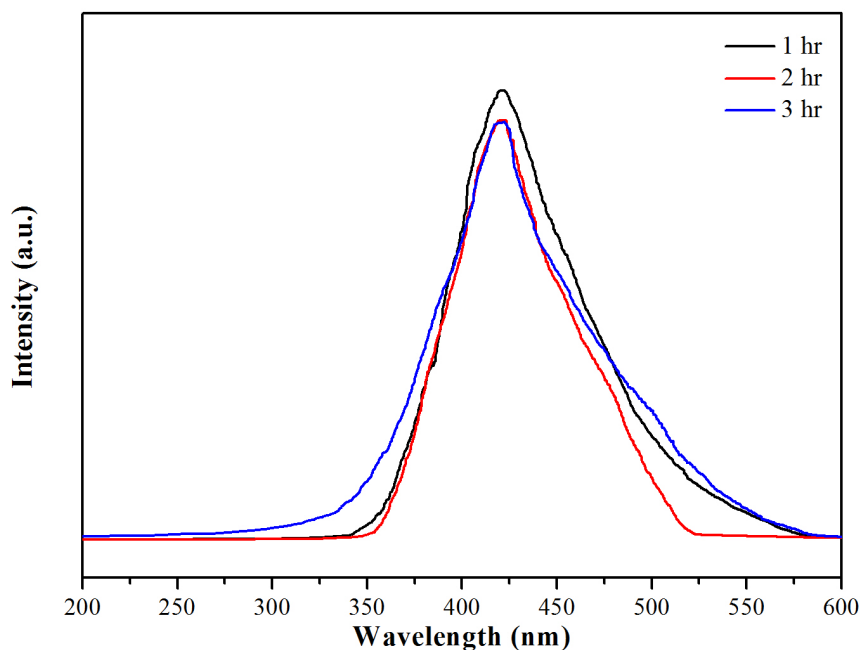


Figure 7 | Fluorescence spectra of a TA-OH<sup>•</sup> solution generated by 1.50 mol% Fe-doped CeO<sub>2</sub> under visible light irradiation.

$$E_{vb}(\text{CeO}_2) = E_g - E_{cb}(\text{CeO}_2) \quad (4)$$

Where  $\chi$  is the absolute electronegativity of the semiconductor ( $\chi$  is 5.56 eV for CeO<sub>2</sub>)<sup>32</sup>,

$E^c$  is the scaling factor relating the hydrogen electrode scale (NHE) to absolute vacuum scale (AVS) ( $\sim 4.5$  eV vs. AVS for 0 V vs. NHE)<sup>32</sup> and  $E_g$  is the band gap energy of CeO<sub>2</sub> (3.00 eV). The calculated CB and VB potentials of CeO<sub>2</sub> are  $-0.44$  and  $2.56$  eV, respectively.

It is proposed schematically in Figure 8 that the photogenerated electron-hole pairs are able to be separated for into trap states in the doped material. The presence of Fe<sup>3+</sup>, as shown in XPS analysis (Figure 1a) may act as electron acceptor (from Fe<sup>3+</sup> to Fe<sup>2+</sup>) and/or hole donor (from Fe<sup>3+</sup> to Fe<sup>4+</sup>) to facilitate charge carrier localisation and hence prolonged separation by trapping at energy levels close to the conduction or valence bands, respectively<sup>33</sup>. Therefore, the Fe<sup>3+</sup> doping could be effective in producing materials that (1) delay electron-hole recombination, thereby increasing the lifetime of the elec-

tron-hole separation<sup>34</sup> as confirmed in PL results and (2) support the charge carrier transfer to the catalyst surface.

*In summary*, Fe-doped CeO<sub>2</sub> catalysts with different iron doping concentrations have successfully been fabricated to produce photocatalytic films by a doctor blade technique. Under visible light irradiation, Fe<sup>3+</sup> doping can significantly increase the photocatalytic activity of CeO<sub>2</sub> towards the degradation of MO, with the best efficiency obtained from a 1.50 mol% iron doping. The enhanced photocatalytic performance upon doping with iron could be ascribed to both the red shift in the light adsorption range and an increased specific surface area, shown in the BET analysis. The presence of Fe<sup>3+</sup> observed from XPS analysis may contributed to the Fe<sup>3+</sup>/Fe<sup>2+</sup> and Fe<sup>4+</sup>/Fe<sup>3+</sup> additional levels in the CeO<sub>2</sub>, and a decrease in band gap energy as a consequence. The PL results confirmed that the iron doping could be effective in delay electron-hole recombination, thereby increasing the lifetime of the electron-hole separation. Since the hydroxyl radical is known to be the key species in photo-

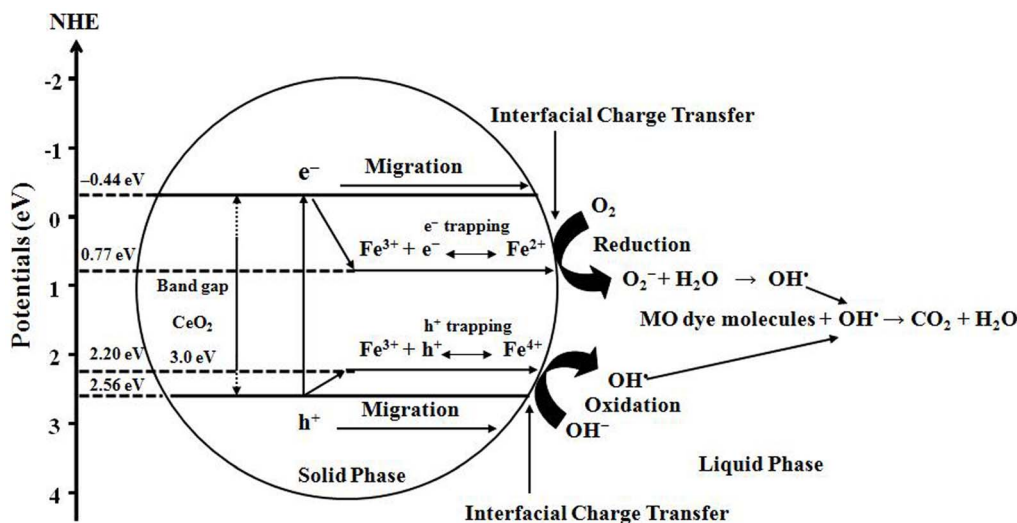


Figure 8 | Proposed mechanism for the photoexcited electron-hole separation and transport processes at the Fe-doped CeO<sub>2</sub> interface under visible light irradiation.



catalytic reactions, thus the PL results proved that the OH<sup>•</sup> adduct TA–OH<sup>•</sup> was formed during the photocatalytic reaction with the presence of catalyst.

## Methods

**Catalysts powder preparation.** Undoped CeO<sub>2</sub> and Fe-doped CeO<sub>2</sub> powders were prepared by the combination of homogeneous precipitation and impregnation methods. Cerium (III) nitrate hexahydrate (Ce(NO<sub>3</sub>)<sub>3</sub>·6H<sub>2</sub>O) and ferric (III) nitrate nonahydrate (Fe(NO<sub>3</sub>)<sub>3</sub>·9H<sub>2</sub>O) were used as precursors. Firstly, a 20 mM of Ce(NO<sub>3</sub>)<sub>3</sub>·6H<sub>2</sub>O in 100 mL of 80% ethylene glycol was prepared and stirred at 50°C until fully dissolved. During this time the colour of solution changed from purple to yellow. Addition of ammonia causes the solution to go purple once again, however after the 12 h aging a turbid yellow suspension was produced, which was then washed with deionised water, then ethanol and then dried in a vacuum oven at 70°C for 24 h. Finally, the prepared CeO<sub>2</sub> samples were calcined at 500°C for 1 h. Fe-doped CeO<sub>2</sub> with different amounts of iron concentration (0.50–5.00 mol%) were prepared by impregnation of undoped CeO<sub>2</sub> powders suspension in water, with the addition of appropriate amount of Fe(NO<sub>3</sub>)<sub>3</sub>·9H<sub>2</sub>O while continuous stirring for 2 h. The sample was then filtered, washed and dried at 70°C overnight and calcined at 500°C for 1 h.

**Catalysts film preparation.** Films of both doped and undoped CeO<sub>2</sub> were prepared by doctor blade technique as described elsewhere<sup>35</sup>. The obtained film was dried in air at 50°C for about 30 min, and further annealed at 500°C for 2 h in order to remove Triton X-100 binder. The films thickness was ~5.0 ± 0.2 μm as measured by profilometer (Supplementary Information 3).

**Film Characterisation.** The films thickness was found to be around 5.0 ± 0.2 μm from Profilometer measurement (Veeco Dektak150). The optical properties of the prepared samples were obtained from a photospectrometer (Shimadzu UV-3600) with integrating sphere attachment. The point of zero charge of catalyst powders was measured with the Zeta potential analysis (Malvern, Zetasizer-NanoS90). The crystalline phase of catalyst film was determined by glancing angle X-ray diffraction (GAXRD, Philips X'pert Materials). The porosity and specific surface area (SSA) were determined using Brunauer, Emmett, Teller (BET) analysis of nitrogen adsorption-desorption data (Quantachrome Autosorp 1 MP). The chemical composition and oxidation state of all materials were studied by X-ray photoelectron spectroscopy (XPS) using Mg X-ray source (MgKα, Kratos Axis Ultra DLD). The binding energy of the adventitious carbon (C 1s) line at 285 eV was used for calibration and the position of other peaks was corrected according to the position of the C 1s signal. The thickness cross-section of the films was measured by scanning electron microscopy (FESEM, JSM-6335F, JEOL). The fluorescence spectra of the generated TA–OH<sup>•</sup> were measured on the fluorescence spectrophotometer at 425 nm (Avantes, AvaSpec-2048 TEC-USB2-2); fluorescence was induced by excitation at 345 nm.

**Photocatalytic testing for the degradation of dyes.** Photocatalytic degradation processes under visible irradiation were investigated using undoped CeO<sub>2</sub> and Fe-doped CeO<sub>2</sub> films through the decolourisation of MO solution with an initial dye concentration of 0.025 mM at pH 5. The adsorption efficiency of MO in dark at different pH value are explained in Supplementary Information 4 and 5. The photoreactor system employed with a halogen lamp (50 watt power) providing a light intensity of ~185 mW cm<sup>-2</sup>. Decolourisation of dye solutions at different time intervals was determined by measuring the change in absorbance maxima of MO at 464 nm via UV-vis spectrophotometer (Shimadzu UV-1800).

**Determination of reactive species (hydroxyl radical, OH<sup>•</sup>).** In order to measure the relative concentration of hydroxyl radicals, the terephthalic acid (TA) fluorescence method was employed in this study owing to the TA can react with OH<sup>•</sup> forming highly fluorescent 2-hydroxyterephthalic acid (TA–OH<sup>•</sup>). The mixture of TA solution was prepared from 5 × 10<sup>-4</sup> molar of TA and 6 × 10<sup>-3</sup> molar of NaOH in DI water. Then, 0.25 g of the 1.50% Fe-doped CeO<sub>2</sub> catalyst was dispersed in 50 mL of the TA aqueous solution. The solution was collected at every one hour during the irradiation procedure in order to estimate the generated TA–OH<sup>•</sup>, which can be detected by fluorescence spectroscopy at 425 nm<sup>36,37</sup>.

- Houas, A. *et al.* Photocatalytic degradation pathway of methylene blue in water. *Appl. Catal. B: Environ.* **31**, 145–157 (2001).
- Ai, L., Zhang, C. & Meng, L. Adsorption of methyl orange from aqueous solution on hydrothermal synthesized Mg–Al layered double hydroxide. *J. Chem. Eng. Data.* **56**, 4217–4225 (2011).
- Lathasree, S., Nageswara, R., Sivasankar, B., Sadasivam, V. & Rengaraj, K. Heterogeneous photocatalytic mineralisation of phenols in aqueous solutions. *J. Mol. Catal. A: Chem.* **223**, 101–105 (2004).
- Chen, L., Tian, J. & Qiu, H. Preparation of TiO<sub>2</sub> nanofilm via sol-gel process and its photocatalytic activity for degradation of methyl orange. *Ceram. Int.* **13**, 3422–3435 (2009).
- Shen, W. *et al.* Photocatalytic degradation for methylene blue using zinc oxide prepared by co-deposition and sol-gel methods. *J. Hazard. Mater.* **152**, 172–175 (2007).
- Kim, S. *et al.* Photocatalytic activity of metal-inserted WO<sub>3</sub> thin films prepared by RF magnetron sputtering. *J. Nanosci. Nanotechnol.* **10**, 7053–7055 (2013).

- Magesh, G., Viswanathan, B., Viswanath, R. P. & Varadarajan, T. K. Photocatalytic behavior of CeO<sub>2</sub>–TiO<sub>2</sub> system for the degradation of methylene blue. *Indian J. Chem. B Org.* **3**, 480–488 (2009).
- Truffault, L. *et al.* Application of nanostructured Ca doped CeO<sub>2</sub> for ultraviolet filtration. *Mater. Res. Bull.* **45**, 527–535 (2010).
- Ho, C., Yu, J. C., Kwong, Y., Mak, A. C. & Lai, S. Morphology-controllable synthesis of mesoporous CeO<sub>2</sub> nano and microstructures. *Chem. Mater.* **17**, 4514–4522 (2005).
- Tuprakay, S. & Liengcharernsit, W. Lifetime and regeneration of immobilized titania for photocatalytic removal of aqueous hexavalent chromium. *J. Hazard. Mater.* **124**, 53–58 (2005).
- Grätzel, M. P. Photoelectrochemical cells. *Nature* **414**, 338–344 (2001).
- Channei, D. *et al.* Photocatalytic activity under visible light of Fe-doped CeO<sub>2</sub> nanoparticles synthesized by flame spray pyrolysis. *Ceram. Int.* **39**, 3129–3134 (2013).
- An, H. *et al.* Iron-coated TiO<sub>2</sub> nanotubes and their photocatalytic performance. *J. Mater. Chem.* **20**, 603–610 (2010).
- Watts, R., Kong, S. & Lee, W. Sedimentation and reuse of titanium dioxide: application to suspended-photocatalyst reactors. *J. Environ. Eng.* **121**, 730–735 (1995).
- Wang, Z. *et al.* Synthesis and characterization of SiO<sub>2</sub>/(PMMA/Fe<sub>3</sub>O<sub>4</sub>) magnetic nanocomposites. *J. Nanosci. Nanotechnol.* **8**, 1797–1802 (2008).
- Andronic, L., Manolache, S. & Duta, A. Photocatalytic degradation of methyl orange: influence of H<sub>2</sub>O<sub>2</sub> in the TiO<sub>2</sub>-based system. *J. Nanosci. Nanotechnol.* **8**, 728–732 (2008).
- Andronic, L., Enesca, A., Vladuta, C. & Duta, A. Photocatalytic activity of cadmium doped TiO<sub>2</sub> films for photocatalytic degradation of dyes. *Chem. Eng. J.* **152**, 64–71 (2009).
- Joshi, K. M. & Shrivastava, V. S. Removal of methylene blue dye aqueous solution using photocatalysis. *Int. J. Nano. Dim.* **2**, 241–252 (2012).
- Yamashita, T. & Hayes, P. Analysis of XPS spectra of Fe<sup>2+</sup> and Fe<sup>3+</sup> ions in oxide materials. *Appl. Surf. Sci.* **254**, 2441–2449 (2008).
- Grosvenor, A. P., Kobe, B. A., Biesinger, M. C. & McIntyre, N. H. Investigation of multiplet splitting of Fe 2p XPS spectra and bonding in iron compounds. *Surf. Interf. Anal.* **36**, 1564–1574 (2004).
- Pradhan, G. K. & Parida, K. M. Fabrication of iron-cerium mixed oxide: An efficient photocatalyst for dye degradation. *Int. J. Eng. Sci. Tech.* **2**, 53–65 (2010).
- Khare, A., Choudhary, R. J., Bapna, K., Phase, D. M. & Sanyal, S. P. Resonance photoemission studies of (111) oriented CeO<sub>2</sub> thin film grown on Si (100) substrate by pulsed laser deposition. *J. Appl. Phys.* **108**, 1–5 (2010).
- Shannon, R. D. Revised effective ionic radii and systematic studies of interatomic distances in halides and chalcogenides. *Acta. Cryst. Sect. A.* **32**, 751–767 (1976).
- Boonprakob, N. *et al.* Enhanced visible-light photocatalytic activity of g-C<sub>3</sub>N<sub>4</sub>/TiO<sub>2</sub> films. *J. Colloid. Interf. Sci.* **417**, 402–409 (2014).
- LÓpez, R. & Gómez, R. Band-gap energy estimation from diffuse reflectance measurements on sol-gel and commercial TiO<sub>2</sub>: A comparative study. *J. Sol-Gel Sci. Technol.* **61**, 1–7 (2012).
- Olad, A., Behboudi, S. & Entezami, A. A. Preparation, characterization and photocatalytic activity of TiO<sub>2</sub>/polyaniline core-shell nanocomposite. *Bull. Mater. Sci.* **35**, 801–809 (2012).
- Bangashi, S. K. & Alam, S. Adsorption of acid blue 1 on activated carbon produced from the wood of *Ailanthus altissima*. *Braz. J. Chem. Eng.* **26**, 275–285 (2009).
- Wang, X. *et al.* Novel BiOCl–C<sub>3</sub>N<sub>4</sub> heterojunction photocatalysts: In situ preparation via an ionic-liquid-assisted solvent-thermal route and their visible-light photocatalytic activities. *Chem. Eng. J.* **234**, 361–371 (2013).
- Nagaveni, K., Hegde, M. S. & Madras, G. Structure and photocatalytic activity of Ti<sub>1-x</sub>M<sub>x</sub>O<sub>2-δ</sub> (M = W, V, Ce, Zr, Fe, and Cu) synthesized by solution combustion Method. *J. Phys. Chem. B.* **108**, 20204–20212 (2004).
- Rawal, S. B., Sung, S. D. & Lee, W. I. Novel Ag<sub>3</sub>PO<sub>4</sub>/TiO<sub>2</sub> composites for efficient decomposition of gaseous 2-propanol under visible-light irradiation. *Catal. Commun.* **17**, 131–135 (2012).
- Xu, Y. & Schoonen, M. A. A. The absolute energy position of conduction and valence bands of selected semiconducting minerals. *Am. Mineral.* **85**, 543–556 (2000).
- Magesh, G., Viswanathan, B., Viswanath, R. P. & Varadarajan, T. K. Photocatalytic behavior of CeO<sub>2</sub>–TiO<sub>2</sub> system for the degradation of methylene blue. *Indian J. Chem.* **48A**, 480–488 (2009).
- Masui, T., Hirai, H. & Imanaka, N. Synthesis of cerium oxide nanoparticles by hydrothermal crystallization with citric acid. *J. Mater. Sci. Lett.* **21**, 489–491 (2002).
- Zhang, Y. & Weber, W. J. Grain growth and phase stability of nanocrystalline cubic zirconia under ion irradiation. *Phys. Rev. B.* **82**, 184105–184112 (2010).
- Belhekar, A. A., Awate, S. V. & Anand, R. Photocatalytic activity of titania modified mesoporous silica for pollution control. *Catal. Commun.* **3**, 453–458 (2002).
- Ishibashi, K., Fujishima, A., Watanabe, T. & Hashimoto, K. Detection of active oxidative species in TiO<sub>2</sub> photocatalysis using the fluorescence technique. *Electrochem. Commun.* **2**, 207–210 (2000).





37. Li, F. T. *et al.* Photocatalytic oxidative desulfurization of dibenzothiophene under simulated sunlight irradiation with mixed-phase Fe<sub>2</sub>O<sub>3</sub> prepared by solution combustion. *Catal. Sci. Technol.* **2**, 1455–1462 (2012).

## Acknowledgments

This work has been supported by Thailand Research Fund (TRF) through the Royal Golden Jubilee (RGJ)-Ph.D Program. National Research University Project under Thailand's Office of Higher Education Commission; Materials Science Research Center, Department of Chemistry, Faculty of Science and the Graduate School, Chiang Mai University are greatly acknowledged. AN would like to thank the Australian Renewable Energy Agency (ARENA) for financial support. The authors would also like to thank the Australian National Fabrication Facility (ANFF) for access to equipment.

## Author contributions

D.C. analysed the data and wrote the manuscript. S.P. and B.I. supervised the project, had given valuable advices on the proceeding of this work, and revised the manuscript. A.N. and J.C. designed the concept and the experiment method of the research. S.U. supported the characterisation of the samples. N.W. had provided valuable suggestions on the selection of

supplementary information. All authors discussed the results and commented on the manuscript at all stages.

## Additional information

**Supplementary information** accompanies this paper at <http://www.nature.com/scientificreports>

**Competing financial interests:** The authors declare no competing financial interests.

**How to cite this article:** Channei, D. *et al.* Photocatalytic Degradation of Methyl Orange by CeO<sub>2</sub> and Fe-doped CeO<sub>2</sub> Films under Visible Light Irradiation. *Sci. Rep.* **4**, 5757; DOI:10.1038/srep05757 (2014).



This work is licensed under a Creative Commons Attribution-NonCommercial-NoDerivs 4.0 International License. The images or other third party material in this article are included in the article's Creative Commons license, unless indicated otherwise in the credit line; if the material is not included under the Creative Commons license, users will need to obtain permission from the license holder in order to reproduce the material. To view a copy of this license, visit <http://creativecommons.org/licenses/by-nc-nd/4.0/>